Engineering Structures 305 (2024) 117715

Contents lists available at ScienceDirect

Engineering Structures

journal homepage: www.elsevier.com/locate/engstruct

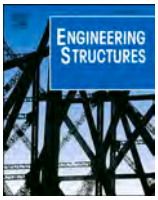

A simplified approach to assess dynamic amplification due to accidental release of formwork traveller during the construction stages of bridges

Javier Sánchez-Haro [a,b,*], Guillermo Capellán [b], Paula Pérez [a], Tommaso Argentini [c]

[a] Department of structural engineering, University of Cantabria, Av. de los Castros 44, Santander 39005, Spain
[b] Arenas&Asociados Ingeniería de Diseño S.L., Marqués de la Ensenada 11, Santander 39009, Spain
[c] Department of Mechanical engineering, Politecnico di Milano, via La Masa 1, 20156 Milano, Italy

ARTICLE INFO

Keywords:
Formwork traveller
Accident
Bioceanic bridge
Chilina bridge, dynamic analysis
Construction stage

ABSTRACT

Construction of bridges by the cantilever method needs to consider the accidental release of the formwork traveller (ARFT) in the design phase. Often this phase is a critical situation that current regulations treat as a static analysis amplified by a dynamic factor due to the difficulty in setting up a model able to simulate the complex interaction between the formwork and the structure in the time domain during the accidental release. To overcome the simplistic approach of the regulations and to avoid the complexity of detailed ARFT modelling, in this research the release of the formwork is modelled as a simple force-time function applied to the bridge. This function has an equivalent effect on the structure as the accidental release, and it has been tuned using experimental tests on a 1:100 scale aeroelastic model of the cable-stayed Bioceanic Bridge. To test the applicability of the proposed time-function the Chilina continuous beam Bridge was also analysed. The article shows that the simplified procedure in the regulations can sometimes underestimate and overestimate dynamic amplification and, thus, a methodology is proposed to carry out the specific dynamic calculation that the regulations suggest for those cases where it is necessary.

1. Introduction

The construction of bridges by the cantilever method needs to consider accidental release of the formwork traveller (ARFT) in the design phase according to the main international regulations. It is often a critical situation from a design point of view because some bridges are less vulnerable once the construction process is complete than during the construction phase. The main international regulations, such as Eurocode [1] in its article 4.12, AASHTO standards [2] in its article 7.4.1, or Setra standards [3] in its article 5.3.3, or national standards such as the Spanish Code [4] in its article 5.3.1., encompass this situation to be evaluated during the bridge design phase. The way of tackling it is common. All regulations propose two approaches to address the problem: a simplified method and a specific dynamic analysis. The simplified method in all of them suggests multiplying the static case of the weight prone to falling by a Dynamic Amplification Factor (DAF) equal to 2, to consider the dynamic effects. If it begins with a static displacement, doubling the initial displacement in the opposite direction results in the initial displacement with its sign reversed. This consideration is based on the 1 degree of freedom (DOF) system response, where, if the load that produces an initial displacement is abruptly released in a dynamic analysis and no damping is considered, the maximum value of the displacement during the system vibration is the initial one but opposite sign [5]. Any element dissipating energy or any duration in the process of the release of the load (not rigorously instantaneous) would result in an amplification of less than 2 in the 1 DOF system, so in theory the regulations establish this value, 2, to guarantee a safe design. Due to the fact that are multi-degree of freedom systems the behavior of bridges is quite different from 1 DOF system. Thus, often the simplified methods in the regulations are not sufficiently accurate as will be shown in this article. In those cases where the simplified method does not yield accurate results, the alternative proposed by the regulations should be employed: a specific dynamic calculation. The challenge lies in the fact that the regulations do not provide specific guidance on this matter, and it is not easy to model the fall of the formwork traveller from a dynamic calculation perspective. This motivated the current research to provide a methodology for conducting dynamic analyses as suggested by the regulations in cases where the simplified method is not sufficient.

Pseudo-instantaneous loads such as impacts on structures [6,7], impulse loads [8,9] and blasts [10,11,12] are currently being

* Correspondence to: Department of the structural engineering of University of Cantabria.
E-mail address: sanchezja@unican.es (J. Sánchez-Haro).

https://doi.org/10.1016/j.engstruct.2024.117715
Received 14 October 2023; Received in revised form 2 February 2024; Accepted 18 February 2024
Available online 24 February 2024

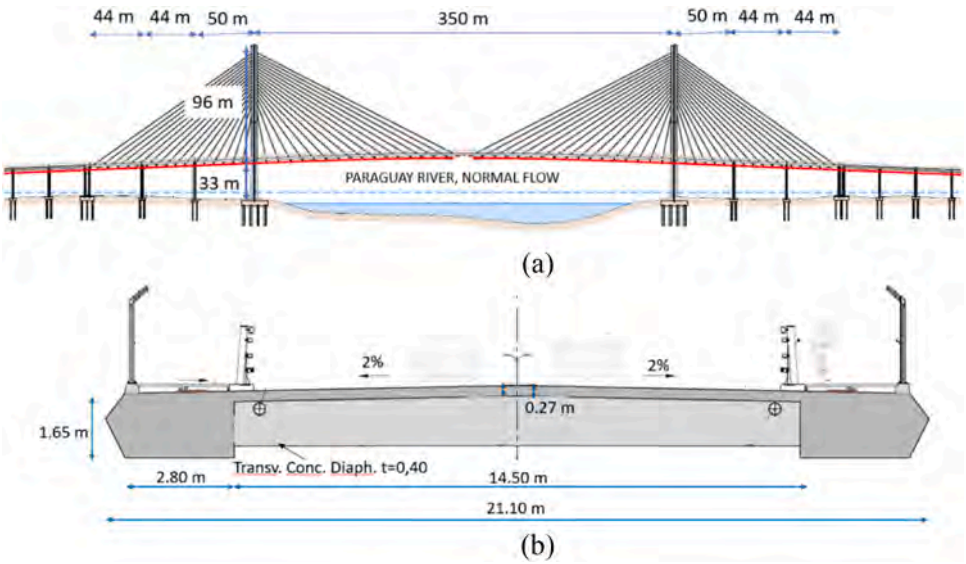

Fig. 1. a: General Geometry of Bioceanic Bridge b: Typical Cross section.

Fig. 2. Infographic of Bioceanic Bridge.

investigated. Bridge vibrations during their construction phase are also subject to study and, in addition to monitoring in real bridges [13,14]. They are studied analytically and numerically, both when their origin is seismic [15,16] and when it is due to wind [17,18,19]. Bridge Vibrations and dynamic amplification in the service phase due to moving loads such as high-speed trains are also under study nowadays [20,21,22,23]. To analyse accidental situations sudden cable failures [24,25] have been researched, however, experimental research has not been found related to ARFT, only to numerical analysis [26]. Research about formwork travellers is being carried out due to the necessity of building larger segments of bridges and the for necessity of more accurate analysis [27, 28], but it is limited to the formwork traveller, not the bridge. Nevertheless, ARFT and its effect on bridges has not been profoundly analysed due to the difficulty of theoretical study and high experimental costs for tests on real structures. Therefore this research aims at providing a simple approach in the time domain to assess more accurately the effects of ARFT with respect to the simplified method in the regulations, while maintaining a low computational and modelling effort. To this end, the ARFT is modelled as a simple force time function applied to the bridge at the traveler location. This function aims at having an equivalent effect on the structure as the accidental release, and it has been tuned using experimental tests on a 1:100 scale aeroelastic model, where the ARFT was simulated.

This article is structured as follows. An Introduction contextualises the problem and discusses the state of knowledge on this subject in the main bridge design regulations. Next, a description is provided of the bridges and formwork travellers analysed in the Materials and Methods section. Then the finite element models, of the two bridges studied (cable-stayed Bioceanic bridge and Chilina continuous beam bridge) are detailed in the "FE Model" section. The "Experimental Tests and Equivalent Force Function For the ARFT" section shows the scale model of the bridge, the scale model of the Formwork Traveller and the calibration process of the equivalent force function. The numerical analysis of all test cases is shown in the Results sections and they are explained in the Discussion section. Finally, the main conclusions of the research are presented.

2. Material and methods

In this section, the bridges and the formwork travellers analysed in this research are described. They were considered according to the most common typologies used in construction of bridges.

2.1. Analysed bridges

There are two typical typologies of bridges where formwork travellers are used as the construction mechanism: cable-stayed bridges and continuous beam bridges. One of each typology was analysed for this article.

First of all, the cable-stayed Bioceanic Bridge, which connects Paraguay and Brazil, with a main bridge span of 350 m, Fig. 1a, was analysed. The other three spans at the beginning and the end of the bridge are 50 m, 44 m and 44 m in length respectively providing stiffness and anchorage to the cables.

Its bridge deck is constructed as a concrete slab of 27 cm of thickness, with two lateral concrete girders, each with a depth of 1.65 m, serving as anchor points for the cables, Fig. 1b. Approximately, every 3 m and in sections with cable stays, a transverse concrete diaphragm of 40 cm thick is provided. The pylons have H form with 96 m height over the bridge deck and 33 m under the deck, approximately. The construction process of this bridge involves building each half of the bridge, finally joining in the centre, Fig. 2, applying a formwork traveller. The maximum cantilever for the Bioceanic Bridge is 175 m right before joining in the middle of its main span.

This bridge is being built nowadays and completion is scheduled in 2025. The Bioceanic Bridge has been designed by Arenas&Asociados, which is also involved in the construction project management.

The second bridge analysed for this research was also designed by Arenas&Asociados, the Chilina Bridge, Fig. 3a. It is a continuous

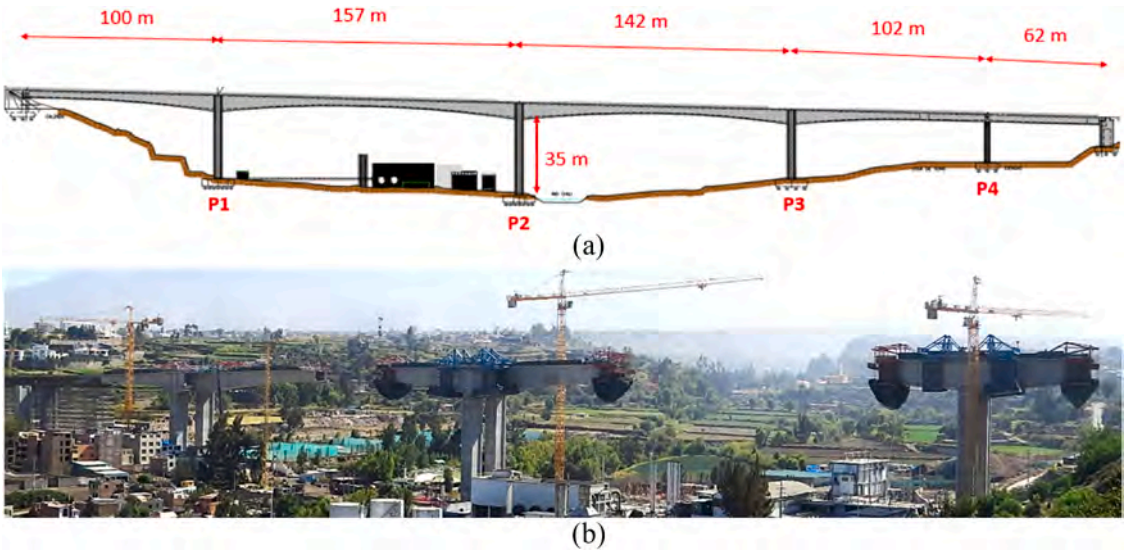

Fig. 3. a: General Geometry of Chilina Bridge b: Photo of Chilina Bridge under construction.

Fig. 4. a: Overhead formwork traveller (OH) b: Underslung formwork traveller (US).

variable-depth beam bridge, built in Peru during the year 2014. It has been detailed in international conferences due to its relevance [29]. This bridge was constructed by cantilever method from the piers, forming T-shaped pier-deck structures, Fig. 3b, till meeting in the middle of each span. The main span, which connects piers 1 and 2, is 157 m in length, which means a maximum cantilever of 78 m during the construction phase. The cross-section of the piers is quasi-rectangular, attaining peak height at pier 2, at 35 m.

2.2. Analysed formwork travellers

There are two main types of formwork traveller: overhead formwork traveller (OH), Fig. 4a, and underslung formwork traveller (US), Fig. 4b. The OH type is placed over the bridge deck, anchoring a cable on the back side of the bridge to equilibrate the assembly. They can be used in both continuous beam, such as the Chilina Bridge, and cable-stayed bridges, such as the Bioceanic Bridge. The US type can only be used in cable-stayed bridges, because they need to be anchored to a cable stay in its front part to achieve stability. This US typology places the carriage under the deck and enables building longer segments than OH. Generally, US type is used in slab-type decks, whereas OH type enables box-sections, although its maximum length of built bridge segment is more limited (5–6 m).

3. FE models

Both the Bioceanic Bridge and the Chilina Bridge were modelled for this research using the finite elements program *Sofistik 2022*, widely used software for dynamic and static modelling of bridges [30,31,32]. The finite element models (FEM) were developed based on the plans provided by the design company Arenas&Asociados and carried out under their supervision. For this reason, the models precisely correspond to the authentic geometry and mechanical properties of both bridges. For the research on the bridges, static analysis, modal analysis and dynamic analysis with direct integration were performed applying appropriate temporal and spatial discretization as in [33] to obtain reliable results.

3.1. Bioceanic bridge

Two phases of the construction process of the Bioceanic Bridge were modelled, which were identified as critical ones during the project design. The first one is termed the *Initial Stage* (IS), Fig. 5a, which is the maximum cantilever just before fixing the deck to one of the piers of the back span. In this situation the self-weight of the formwork traveller placed at the end of the cantilever (FT- Static Case) is supported by the bending moment of the pylon. Specifically, the most critical section of the pylon is located at the height of the deck. For this reason, the Pylon

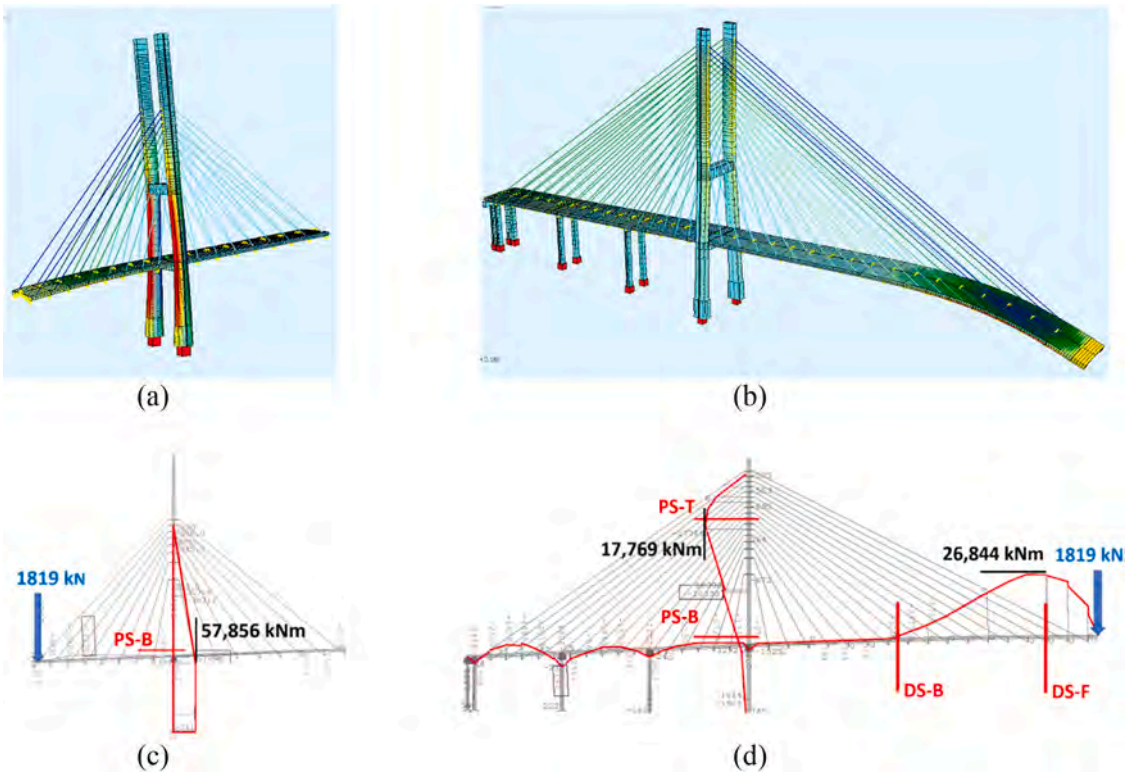

Fig. 5. a: Initial Stage (IS). Displacement shape due to FT-Case. b: Last Stage (LS). Displacement shape due to FT Case. c: Bend. M. diagram due to FT-Case (IS). Checked Section. d: Bend. M. diagram due to FT Case (LS). Checked Sections.

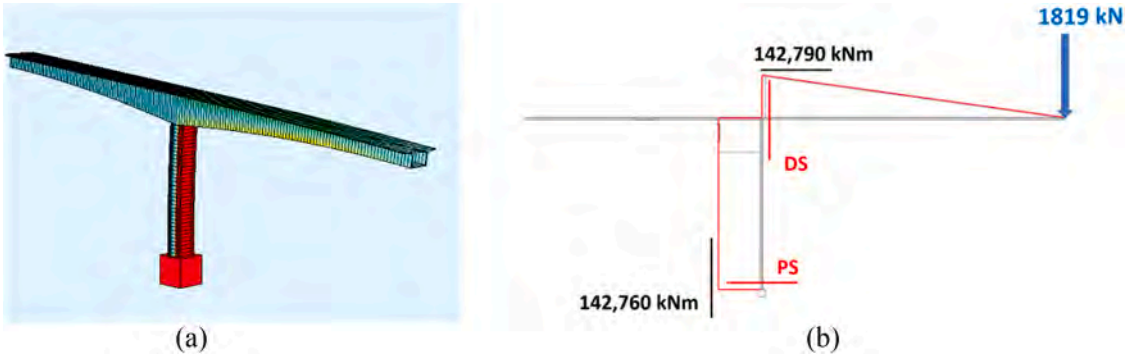

Fig. 6. a: Chilina FEM. b: Bending M. diagram (FT-Case). Checked Sections.

Section-Bottom (PS-B) is checked, Fig. 5c.

The second phase analysed is termed the Last Stage (LS), which is characterized by having the absolute maximum cantilever. It happens just before joining with the other half of the bridge, Fig. 5b. In this situation for the FT-Case, the most loaded deck section is close to edge of the cantilever and for the pylon, its upper part, Fig. 5d. Thus Pylon Section-Top (PS-T), and the Deck Section-Front (DS-F) are checked. Additionally, Deck Section-Back (DS-B) was also checked because define the section from which internal forces are theoretically negligible.

3.2. Chilina bridge

Only one phase of the construction process was modelled in the Chilina Bridge, because only one was identified as critical for the ARFT. The phase modelled is the one with the maximum cantilever just before joining with the other half from the next pier, Fig. 6a. Under the FT-Static Case load, identical to the Bioceanic Bridge, both the deck section closest to the pier (DS) and the pier section fixed at the foundation (PS) are the most critical sections due to the bending moments so they were selected for verification, Fig. 6b.

3.3. Dynamic analysis

All dynamic analyses performed on the finite element models described earlier have been linear analyses with direct time integration based on the Newmark method. The time step used for the analyses is set to 0.001 s. Convergence for each step is based on the residual force concept, which is the difference between external and internal forces. It is considered to have converged if the difference between them is less than the tolerance. A tolerance of 0.1% has been used for all analyses. Sofistik performs this process automatically. All the parameters selected for dynamic analysis were thoroughly examined to ensure that they do not exert any influence on the results. The showcased Finite Element (FE) models in the article corresponds to the actual FE models employed in both Bioceanic and Chilina bridge design.

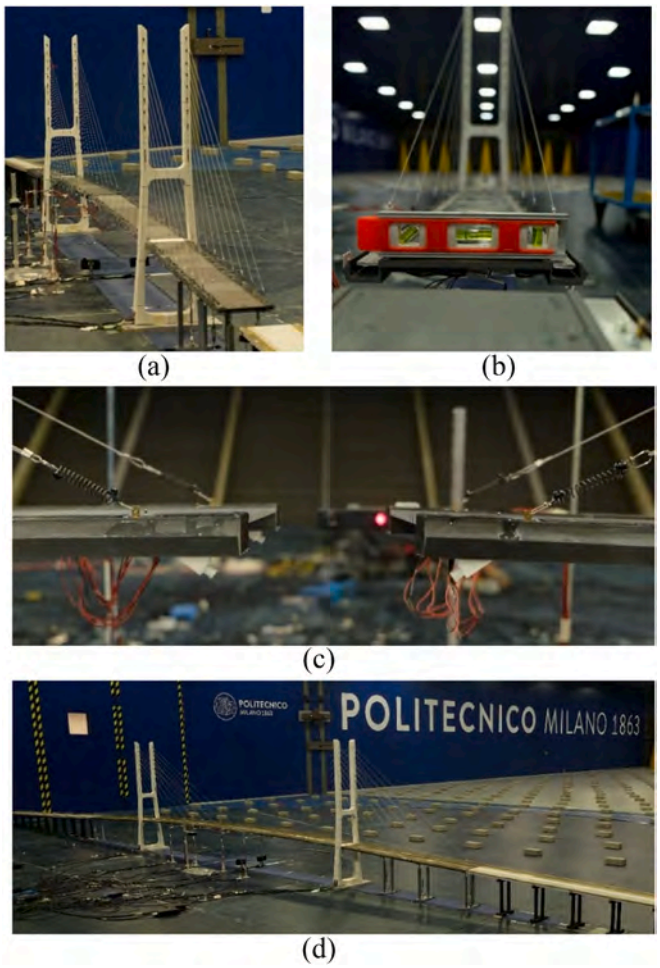

Fig. 7. a: General perspective of the scale model. a: Pylon detail. b: Model construction. c: Edge of the cantilever without connection.

4. Experimental tests and equivalent force function for ARFT

4.1. Aeroelastic model

A 6 m long scale model was developed (geometric scale 1:100) of the Bioceanic Bridge (SMBB) to calibrate the force-model based on experimental tests. This model was available since it was previously used for wind tunnel tests, to assess the aeroelastic performances of the construction stages, which can be critical for bridges, [34].

For the present research, tests involved free vibration tests and ARFT simulation during the maximum cantilever phase (LS). The full-scale model of the Bioceanic Bridge was developed in Politecnico di Milano, Fig. 7, where wind tunnel tests and ARFT tests were carried out.

Different sensors were placed for the monitoring of the SMBB to obtain the data from the tests. Fig. 8a shows the location of the accelerometers (blue), the location of the inclinometers (green) and the verification point (M21) to measure the displacement by laser (red). In addition, Fig. 8b shows the load cell used to measure the weight of hanging objects to perform the ARFT tests.

4.2. Test description

Three different tests were defined with the main aim of the article in mind: Free Vibration after initial displacement (FV), Formwork Traveller Accidental Release-Overhead (ARFT-OH) and Formwork Traveller Accidental Release-Underslung (ARFT-US). The initial static displacement of the whole tests was the same in order to compare the results.

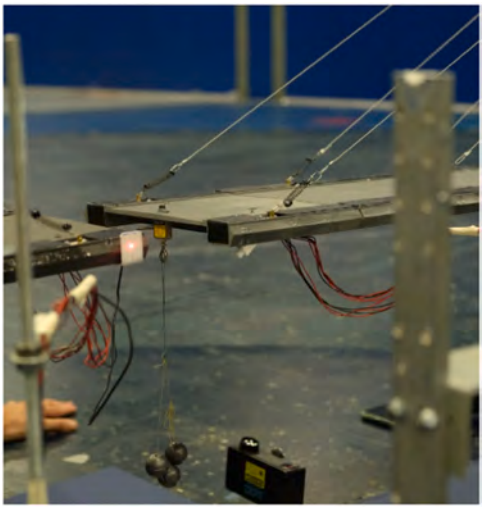

Fig. 9. -Free Vibration test (FV).

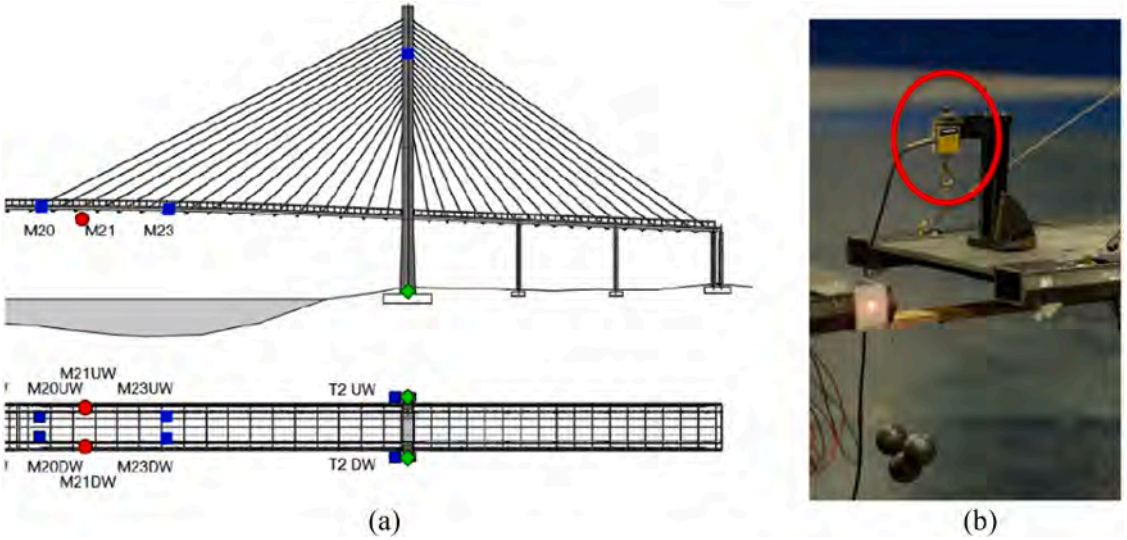

Fig. 8. a: Monitoring devices on model. b: Load cell.

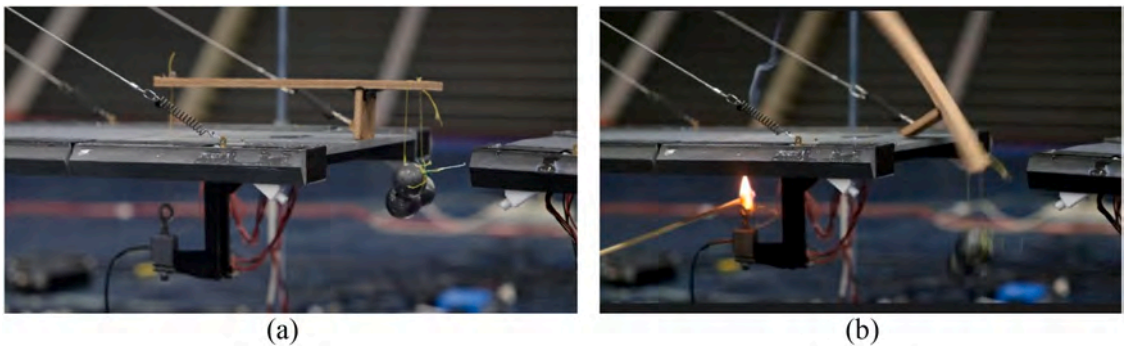

Fig. 10. a: Overhead test (ARFT-OH). Initial instant. b: Overhead test (ARFT-OH). Overturning.

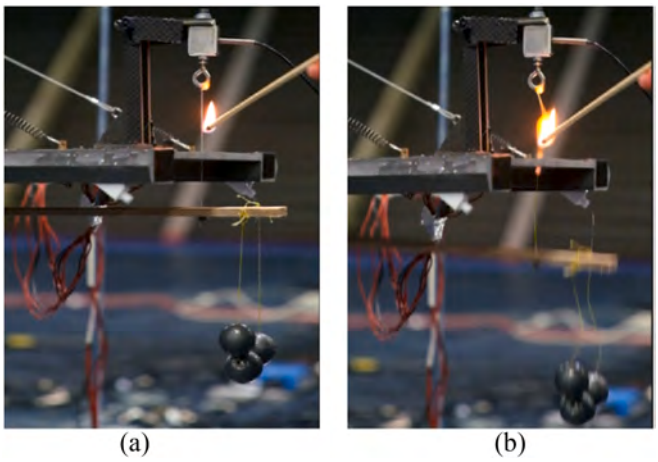

Fig. 11. a: Overhead test (ARFT-US). Initial instant. b: Overhead test (ARFT-US). Instant of release.

A weight was placed at the end of the cantilever during the FV tests, Fig. 9, held from the load cell by a thread, which was burned to simulate a sudden a variation of the load due to the accidental release. The displacement of point M21 was recorded before and after cutting the thread by the laser during the free vibration of the structure. Due to the sudden removal of the load, this test should give a DAF = 2 according to the simplified method in the regulations.

During the ARFT-OH tests the formwork traveller and the weight that models the segment under construction are placed on the deck, Fig. 10a. When the rear thread is burned, the formwork traveller tips over, Fig. 10b. The displacement of point M21is also registered throughout the whole process.

In the last of the three tests (ARFT-US), the formwork traveller and the weight that models the segment under construction are placed under the deck held by the front thread from the load cell placed at the edge of the cantilever, Fig. 11a, and it was also burned to induce the drop, Fig. 11b.

Both the ARFT-OH tests and the ARFT-US tests aim to evaluate the importance of the difference regarding the removal of the instantaneous load (FV test). The longer the time the formwork traveller takes to tip over, the less instantaneous the load release is and thus the greater the expected difference compared with the FV test. The properties of both the OH and the US formwork travellers used for the experimental tests are defined below.

4.3. Definition of formwork travellers used in test

There are different kinds of formwork traveller according to their size, their mechanical properties and the weight of the bridge segment that they have to build. As the number of cases is very large, for this research, it was decided to model formwork travellers at the lower limit. This means that any real formwork traveller would take more time to overturn and finally fall than the model ones. The features of a real formwork traveller are detailed to provide a reference. The weight of the formwork traveller (SW_{FT}) considered for the design of the Bioceanic Bridge was 720 kN. The weight of segment (SW_S) in construction was 1100 kN, thus the total weight (SW_T) that could have dropped in an accidental situation was 1820 kN. Thus, the SW_{FT} represented 40% of the potential drop weight. The net force of SW_{FT} is located more centrally in the deck than the net force of SW_S, so the less is the percentage of the weight of the formwork traveller compared to the SW_T, the larger the eccentricity "*e*" would be from the net force of SW_T, Fig. 12a. Thus, the larger eccentricity "*e*", the faster the overturning and drop of the formwork traveller would be in an accidental situation, Fig. 12b.

The geometry of both the cantilever OH and the US formwork traveller used in the tests are shown in Fig. 13a and b, respectively.

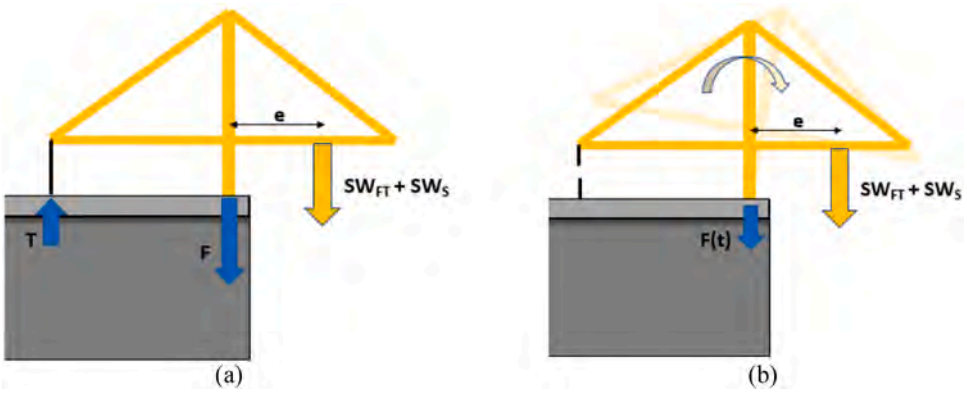

Fig. 12. a: Static Equilibrium b: Formwork Traveller Accidental Release (ARFT).

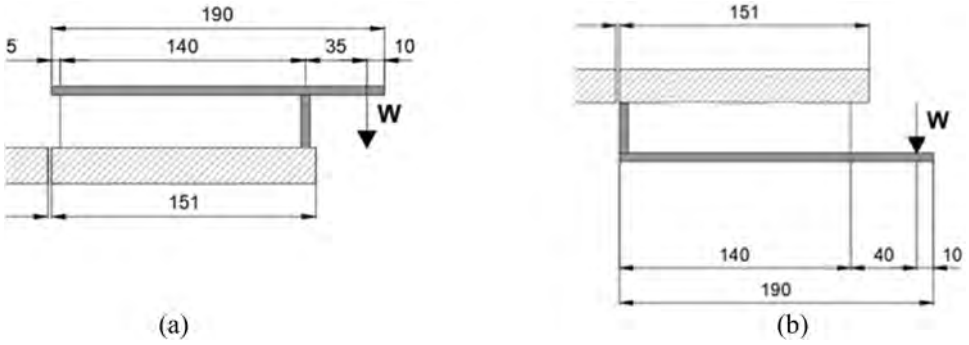

Fig. 13. a Experimental OH geometry. b Experimental US geometry.

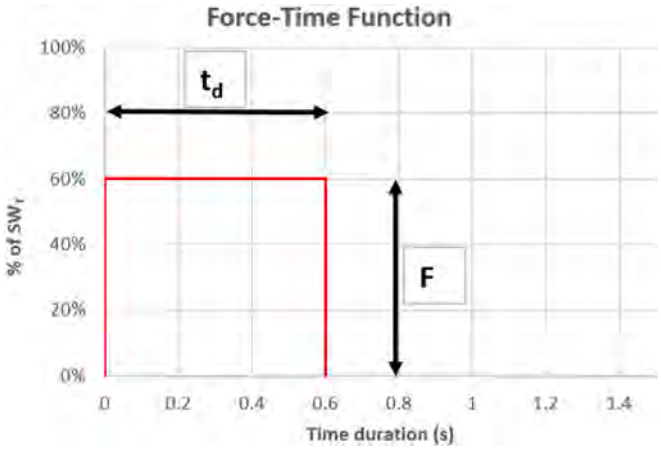

Fig. 14. Force-Time function parameters.

The weight of the formwork traveller used in the tests was 13.5 g, and the weight of metallic balls representing the segment under construction was W = 168.5 g, which represents the 1820 kN that was the design value during the design of the Bioceanic Bridge in real scale (1/10^6). According to the weight distribution in the scale model, SW_{FT} represents 7.5% of the SW_T, unlike the 40% in the project phase. In addition, the rotational inertia of the formwork traveller under test was 7 times lower than the real formwork traveller of the Bioceanic Bridge. Thus If the overturning occurs faster due to the fact that the eccentricity "*e*" is larger and the rotational inertia is smaller, the results obtained from tests will be conservative (closer to FV results), on the safe side. Finally, it is worth noting that actual formwork travellers have a deck connection system always based on more than one cable for safety reasons, so a failure process of the anchoring system would not be immediate and would dissipate energy. In the experimental tests, this effect has deliberately not been taken into account, following the same approach as when defining a small rotational inertia and a large eccentricity to ensure that the research results are conservative and can be confidently applied.

4.4. *Calibration of the equivalent force time function*

The tests were performed at Politecnico di Milano and they were useful to calibrate both the behaviour of the Bioceanic Bridge in FV (mass, stiffness, frequency, modes, damping…) and the force exerted on the bridge by the formwork traveller during the overturning. The aim was to assess how close the ARFT test was to the hypothesis of the instantaneous load release. The calibration of the FEM was performed in LS phase of the Bioceanic Bridge. The check point (M21) is placed 25 m (in real scale) from the edge of the cantilever, Fig. 8a. This calibration consists of the adjustment of properties such as mode displacement, frequency, mass, stiffness and damping ratio (*D* parameter). Only the damping calibration is shown in this article because the other ones are not relevant for this research. However, the calibration of the Force-Time function during the overturning is shown in detail. Assuming the

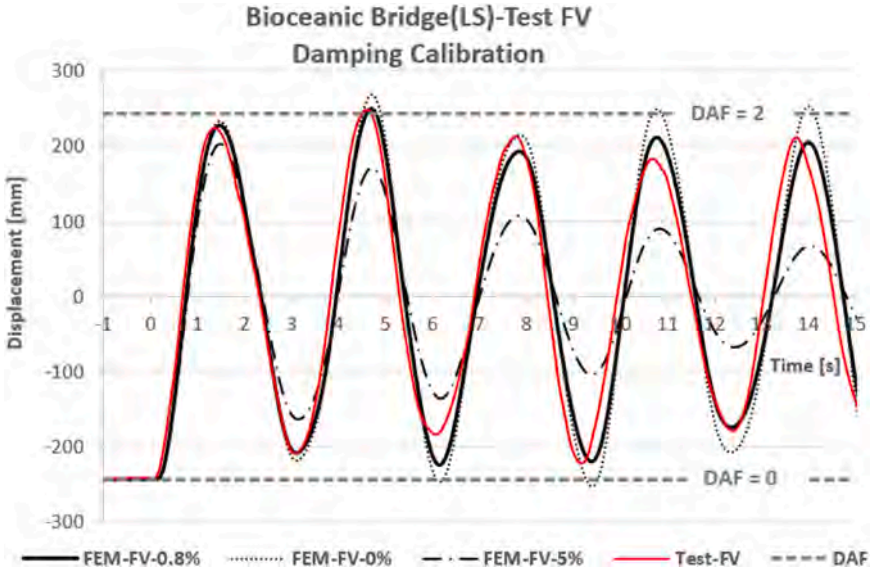

Fig. 15. Displacement vs Time diagram at check point in case FV.

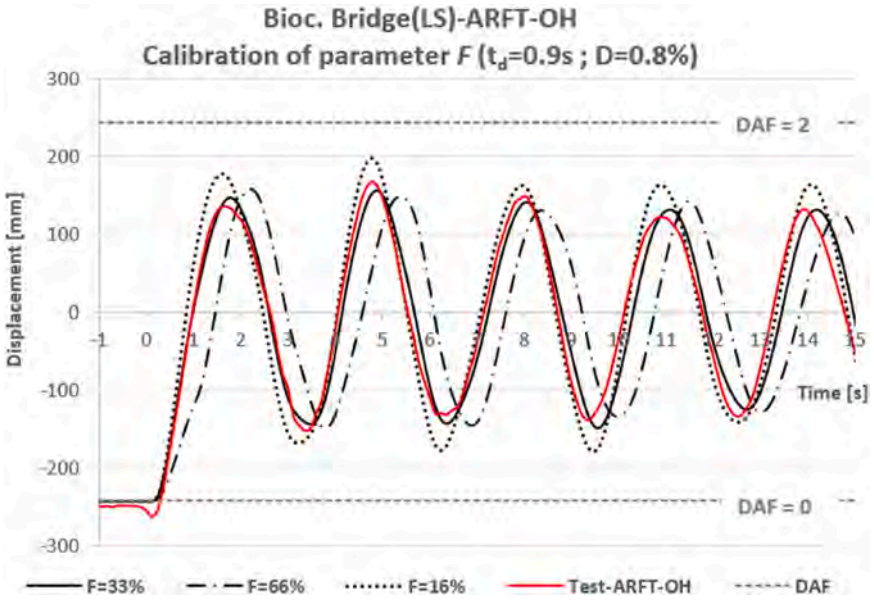

Fig. 16. Displacement vs Time diagram at checkpoint in case ARFT-OH (t_d=0.9 s D=0.8%).

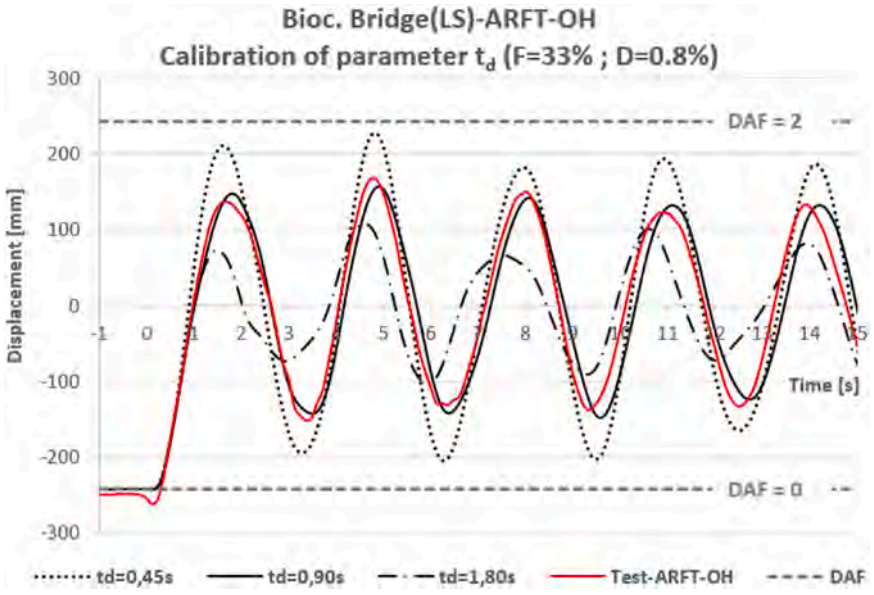

Fig. 17. Displacement vs Time diagram at checkpoint in case ARFT-OH. F= 33% D= 0.8%.

hypothesis of rectangular shape for the Force-Time function, the calibration seeks the percentage of the total dropped weight (SW_T) borne by the deck (F parameter) and how long this force acts for (t_d parameter), Fig. 14.

Firstly, damping calibration was performed, Fig. 15, in the FV test. The measured results of the check point in the LS phase (solid red line) of the Bioceanic Bridge are compared with the FEM results for different damping values (black lines); the dotted black line represents the FEM results for 0% damping, the solid black line represents 0.8% damping and the dashed-dotted line represents 5% damping. This graph of results, and the next ones that follow, show two horizontal grey dashed lines which represent displacement that produces DAF = 0 (initial static value) and DAF = 2 (maximum amplification defined by the simplified method in the regulations).

As can be seen in Fig. 15, the 0.8% damping value matched the results between experimental test and FEM. The instant when the displacement is null fits between the scale model and the FEM results. Thus the frequencies match in all cases and for 0.8% damping, the displacement amplitude of both curves is quite similar (FEM also reproduces the second peak slightly higher than the first one). Based on these results the value of $D = 0.8\%$ is identified as the damping of the scale model. Fig. 15 also shows that the maximum displacement of the FV test is close to the DAF = 2 line for any damping value at the beginning of the test as predicted by the simplified method in the regulations. Once the FEM of FV is calibrated, the next step is to calibrate the values of parameters F and t_d for the ARFT-OH test. Due to the fact that both of them are initially unknown, the t_d parameter is estimated from the camera filming the experimental tests. This parameter value was 0.9 s approximately in real scale (this value will be verified later). Thus, with damping of 0.8% and time duration of 0.9 s, the F parameter is obtained from the ARFT-OH test. The FEM results for force values of 300 kN (F=16%, dotted black line), 600 kN (F=33%, solid black line) and 1200 kN (F=66%, dashed-dotted black line) and the results of the ARFT-OH (red line) experimental test are shown in Fig. 16.

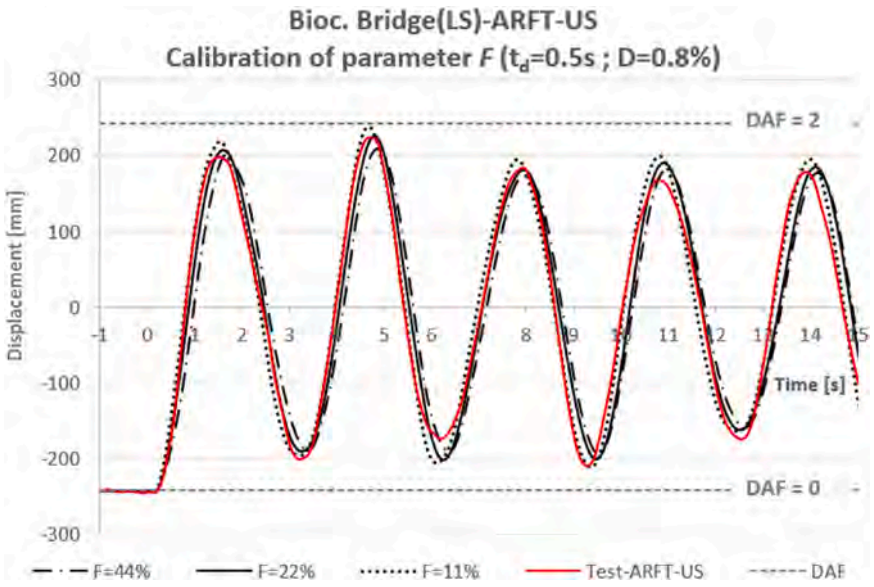

Fig. 18. Displacement vs Time diagram at checkpoint in case ARFT-UD. td = 0.5 s D= 0.8%.

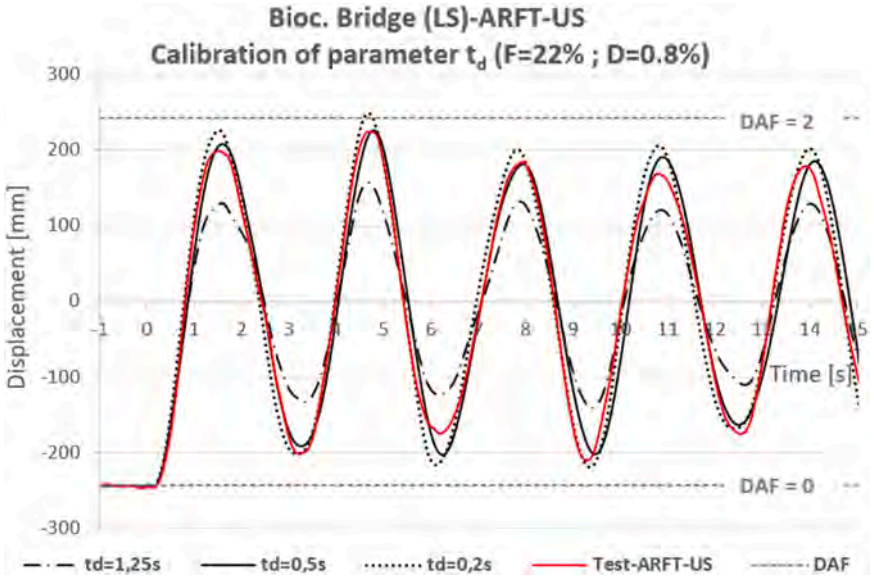

Fig. 19. Displacement vs Time diagram at checkpoint in case ARFT-UD. F= 22% D= 0.8%.

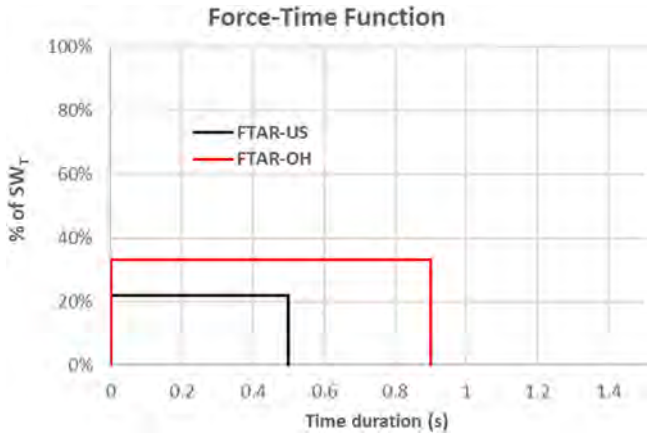

Fig. 20. Force-Time functions for ARFT-OH and ARFT-US cases.

According to the results shown in Fig. 16 the force value shows the influence of parameter *F* at the instant when the maximum displacement is obtained. The previous graph also proves that the curve of a force of 600 kN (*F*=33%) strongly fits with the experimental results. It must be highlighted that the ARFT-OH test shows the maximum displacements is clearly distant from the DAF = 2 line. Thus the hypothesis of instantaneous load release does not to match properly with the reality of this overturning process. In order to check parameter t_d, a calibration has been performed using different values of parameter t_d for the same 600 kN force value and the same 0.8% damping value; in this way the sensitivity of parameter td is analyzed. Fig. 17 shows the different FEM results for this parameter: $t_d = 0.45$ s (15% of the fundamental period, dotted black line), $t_d = 0.90$ s (30% of the fundamental period, solid black line), and $t_d = 1.80$ s (60% of the fundamental period, dashed-dotted black line). The solid red line shows the experimental results of the ARFT-OH test.

As can be seen at Fig. 17, the correct value of td = 0.90 s is confirmed. A similar process of ARFT-OH test is repeated for the ARFT-

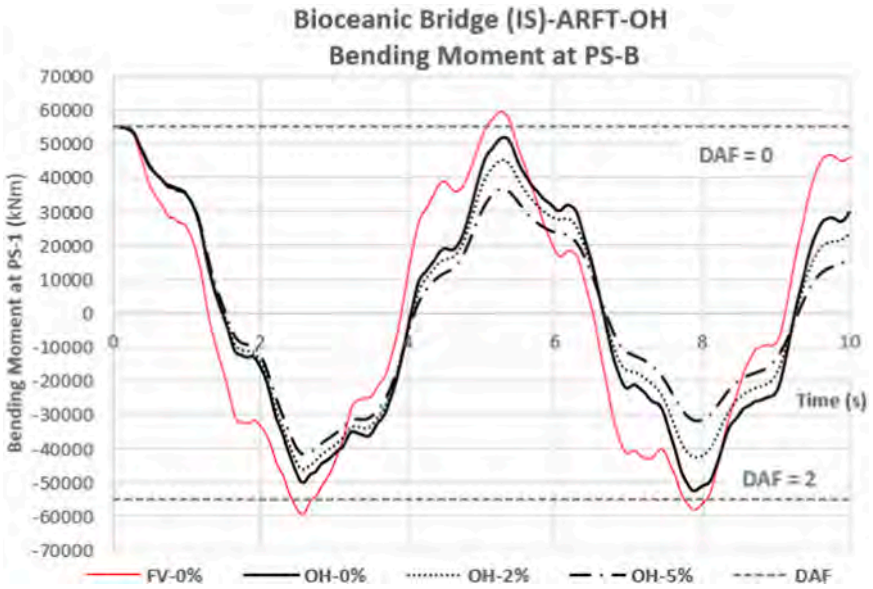

Fig. 21. Bending Moment vs Time diagram at section PS-B in case ARFT-OH over Bioceanic Bridge (IS).

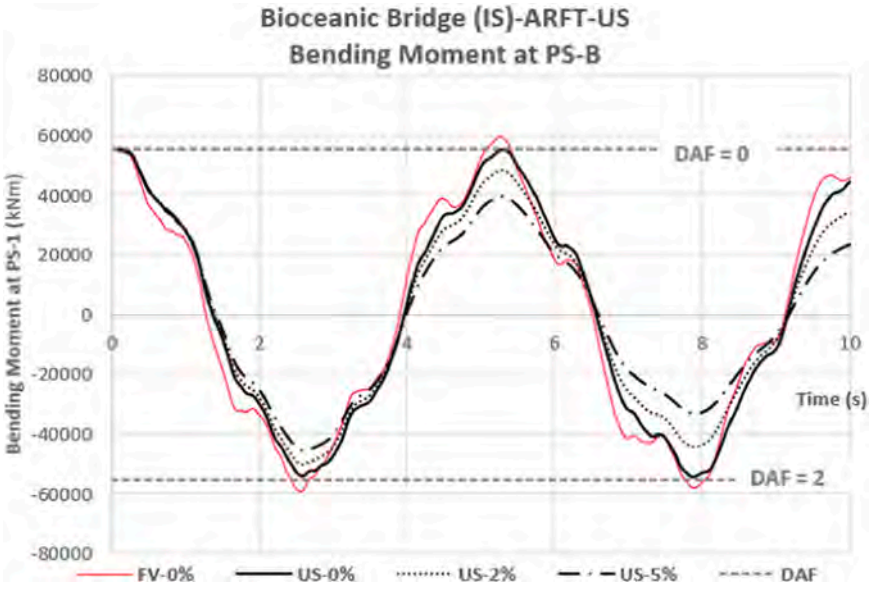

Fig. 22. Bending Moment vs Time diagram at section PS-B in case ARFT-US over Bioceanic Bridge (IS).

US test. It was observed from the filming camera that parameter t_d is around 0.5 s for the ARFT-US test. Additionally, the damping of the scale model was fixed at 0.8%, so the FEM results are obtained for different values of parameter F for the ARFT-US test. Fig. 18 shows the results of the experimental test (solid red line) and FEM results for the force values of 200 kN (F=11%, dotted black line), 400 kN (F=22%, solid black line), and 800 kN (F=44%, dashed-dotted black line).

The displacement curves shown in Fig. 18 are quite similar, but taking into account the maximum displacement peak, the best fit for a force value is for 400 kN (F=22%). Comparing both Fig. 16 and Fig. 18, it can be concluded that the maximum displacement is closer to the DAF = 2 line in the ARFT-US than in the ARFT-OH, which means that ARFT-US is closer to a sudden drop. In an analogous way to what was performed for the ARFT-OH test, the influence of parameter t_d was checked once the damping value (0.8%) and the percentage parameter ($F = 22\%$) were determined. The results of the ARFT-US experimental test (solid red line) and FEM results for three different values of parameter t_d are shown in Fig. 19: $t_d = 0.2$ s (7% of the fundamental period, dotted black line), $t_d = 0.5$ s (16% of the fundamental period, solid black line) and $t_d = 1.25$ s (40% del fundamental period, dashed-dotted black line).

As can be seen in Fig. 19, the curve corresponding to the value of $t_d = 0.5$ s strongly matches with experimental results. The influence in results of the parameter t_d is larger than the parameter F obtained before. Based on the whole calibration process, it can be concluded that during the ARFT-OH test a force of 600 kN (F=33%) is exerted on the deck during 0.9 s ($t_d = 0.9$ s), while during the ARFT-US test a force of 400 kN (F=22%) is exerted on the deck during 0.5 s ($t_d = 0.5$ s), Fig. 20.

Finally, and considering these values as very conservative ones obtained with a higher eccentricity of bigger loads and lower rotational inertia than in real cases, the authors propose the following considerations in order to generalize this analysis for other bridges and other formwork travellers: a) Assume the type of bridge has no influence on the parameters obtained, which means the drop is fast enough to be approximately the same independently of the bridge. b) The force value

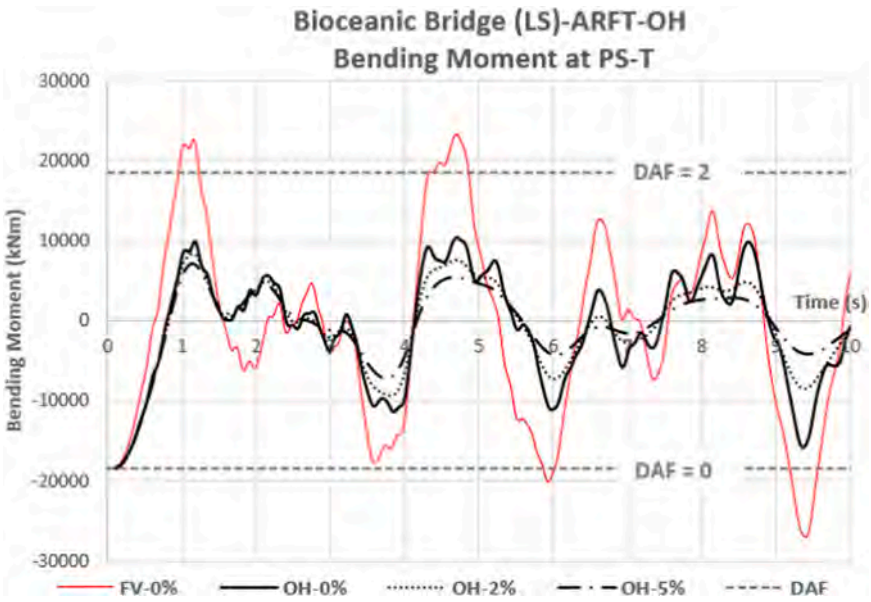

Fig. 23. Bending Moment vs Time diagram at section PS-T in case ARFT-OH over Bioceanic Bridge (LS).

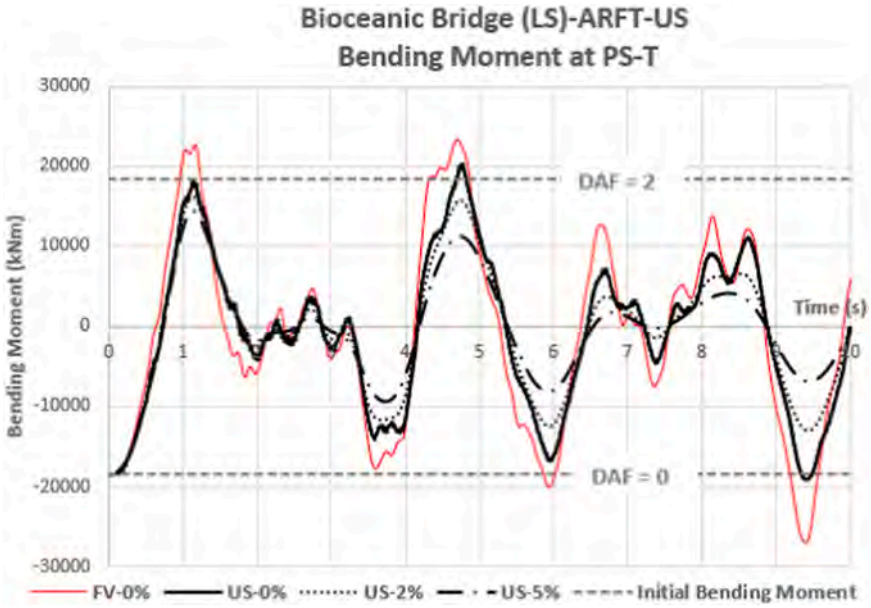

Fig. 24. Bending Moment vs Time diagram at section PS-T in case ARFT-US over Bioceanic Bridge (LS).

exerted on the deck must be estimated around 33% of SW_T when the formwork traveller is OH type and around 20% for the US type. c) The duration of the applied force on the deck can be considered as constant for each type of formwork traveller. This assumption is because the heavier the formwork traveller is, the larger the overturning moment is, and also the larger the rotational inertia is. Thus both effects would be mostly compensated. Thus, the duration can be considered as constant with values of 0.9 s for OH formwork traveller type and 0.5 s for US type. d) These values can be considered as conservative ones due to the mechanical properties of the formwork travellers used in the experimental tests. e) The force functions must be applied in the opposite direction to the movement produced by the initial displacement in a dynamic analysis.

5. Results

Once the Force-Time function was obtained from the calibration analysis of the Bioceanic Bridge, dynamic calculations were performed by using direct integration in all FEM analysis described in Section 3. The aim of this analysis was to study how the formwork traveller influences internal forces in comparison to the results of the simplified method in the regulations. Three damping values were analysed: 0% (solid black line), 2% (dotted black line) and 5% (dashed-dotted black line), this last value is the most realistic in concrete bridges exposed to a critical situation of collapse such as the ARFT. For comparison the results obtained in the FV case (solid red line) are also shown.

5.1. Bioceanic bridge. Initial stage (IS)

Bending moment results for IS phase are shown at section PS-B in the

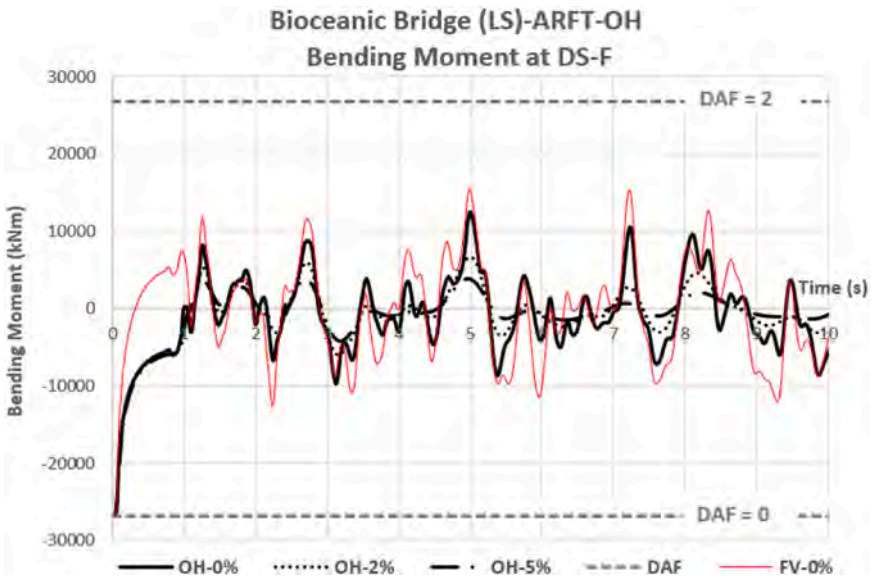

Fig. 25. Bending Moment vs Time diagram at section DS-F in case ARFT-OH over Bioceanic Bridge (LS).

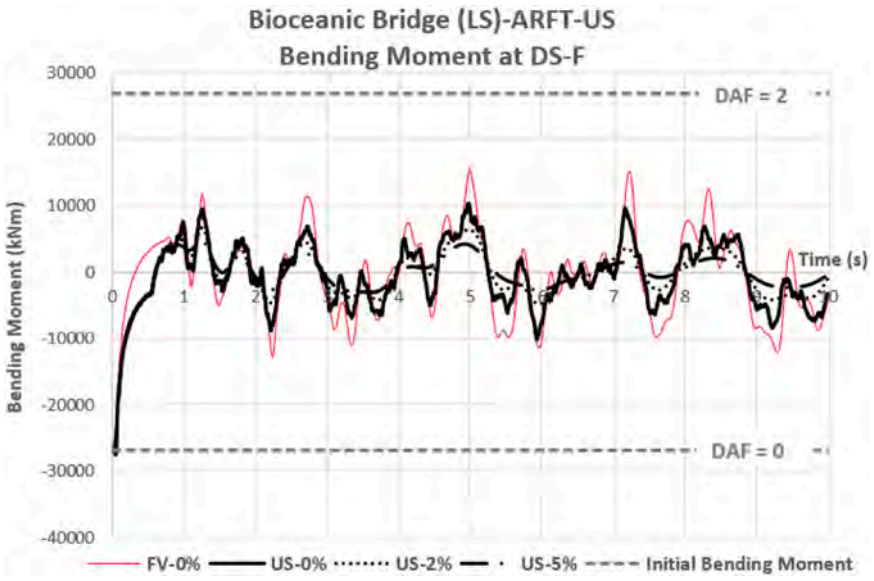

Fig. 26. Bending Moment vs Time diagram at section DS-F in case ARFT-US over Bioceanic Bridge (LS).

ARFT-OH test, Fig. 21, and ARFT-US, Fig. 22.

5.2. Bioceanic bridge. Last stage (LS)

Bending moment results for LS phase are now shown at section PS-T, Fig. 23 and Fig. 24, for section DS-B, Fig. 25 and Fig. 26, and for section DS-F, Fig. 27 and Fig. 28, for the ARFT-OH and ARFT-US tests, respectively.

5.3. Chilina bridge

Bending moment results for the Chilina Bridge for section DS, Fig. 29, and for section PS, Fig. 30, are shown in the ARFT-OD case (ARFT-US only applies in cable-stayed bridges).

6. Discussion

The maximum values obtained for DAF in accordance with the internal forces analysed in Section 5 are shown in Table 1.

The results in Table 1 for the FS/DS-B section show, as per the spirit of the regulations, that the simplified method should not be applied to sections where, in the static case, there are no significant internal forces. If we compare the bending moments from the static case, which are practically negligible, with those derived from the vibration analysis, deceptively large DAF values can arise (DAF in FS/DS-B in FV = 7.93 >> 2). This is because, even if the DAF is high, the bending moments during vibration is small compared to the bending moments from self-weight in deadload dominated structures, as is the case with cantilever-constructed bridges. It would only make sense to consider these sections in live-load structures. Therefore, the FS/DS-B section is omitted from the subsequent analysis. Thus, based on the results shown in Table 1 it must be highlighted that the DAF values obtained for bending moments in the FV case are significantly greater than 2 (Fig. 23, Fig. 24 and Fig. 30) in sections FS/PS-T and PS. This is because the maximum value possible in a 1 DOF system is DAF = 2, (for both displacements and internal forces). However, when the structure has more than one mode

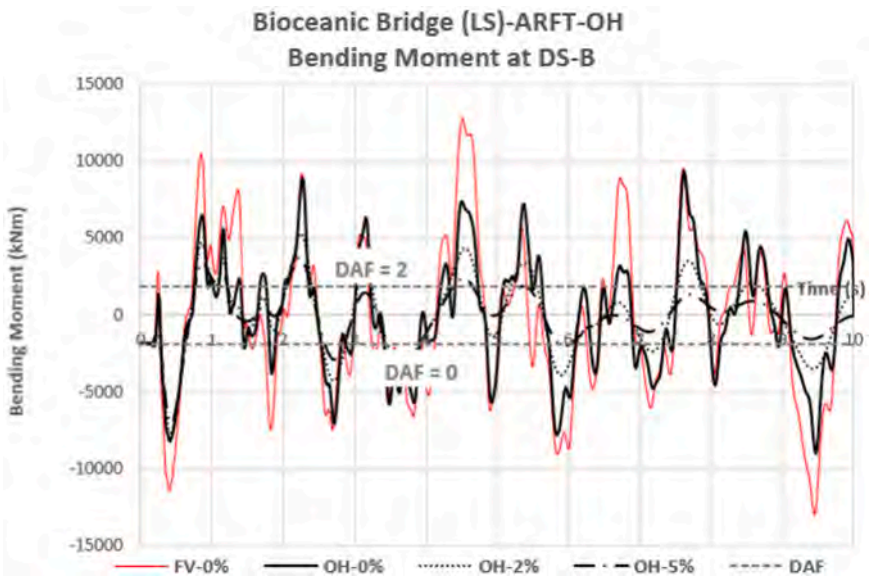

Fig. 27. Bending Moment vs Time diagram at section DS-B in case ARFT-OH over Bioceanic Bridge (LS).

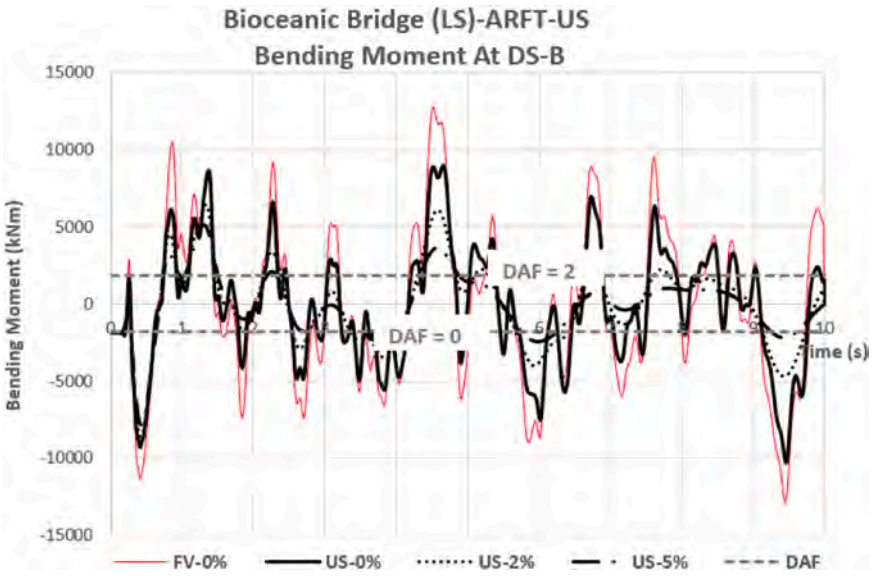

Fig. 28. Bending Moment vs Time diagram at section DS-B in case ARFT-US over Bioceanic Bridge (LS).

of vibration, like a bridge, DAF= 2 is not necessarily the maximum amplification factor for internal forces. Regarding displacement, results of the DAF value are close to 2 (Fig. 15). The principal reason is because the total displacement of a point is mainly generated by the contribution of a single mode, the fundamental one, and thus, the behavior of that displacement is quite similar to a 1 DOF system. Nevertheless, the internal forces are not generated by a predominant mode of vibration in the total summation of a section. As a consequence, it is not possible to ensure that internal forces at the initial instant are the maximum combination of the internal forces that each mode produces throughout the vibration process. That combination can produce larger internal forces than the initial ones, both positive or negative. Thus, a DAF > 2 and a DAF < 0 can occur regarding internal forces. On the other hand, it is important to notice in section DS-F that the opposite happens, Fig. 25 and Fig. 26. Even for the FV case, the bending moment is far from the DAF $= 2$ line, so using this value would oversize the section. However, it can be seen in Table 1, that considering the effects of ARFT, both OH and US with a damping of 5%, the value of DAF $= 2$ is not overpassed and some cases like in section FS/DS-F can have a lot leeway. Additionally, it is interesting to analyze the Dynamic Reduction Factor (DRF) for cases defined in Section 5. These values of DRF are shown in Table 2. The DRF factor indicates the reduction of ARFT compared with the FV case, both for OH and US. The DRF was also compared for the cases of OH and US, with a 5% damping, to quantify the difference between the ARFT-OH and ARFT-US cases.

According to the results shown in **Table 2**, it can be concluded that ARFT does not have similar effects in different situations. In OH cases with a 5% damping, the reduction obtained compared to the FV case is between 25% and 70%, meanwhile for the same characteristics for US, the reduction is in between 31% and 77%. Thus a dynamic analysis has to be performed in every case to know the real amplification.

Lastly, based on the last column in **Table 2**, it can be concluded that the OH formwork traveller is more effective in reducing the internal forces under any situation than the US framework. However all this gain is also variable, from 8% for the IS/PS-B section to 51% for the FS/PS-T section of the Bioceanic bridge.

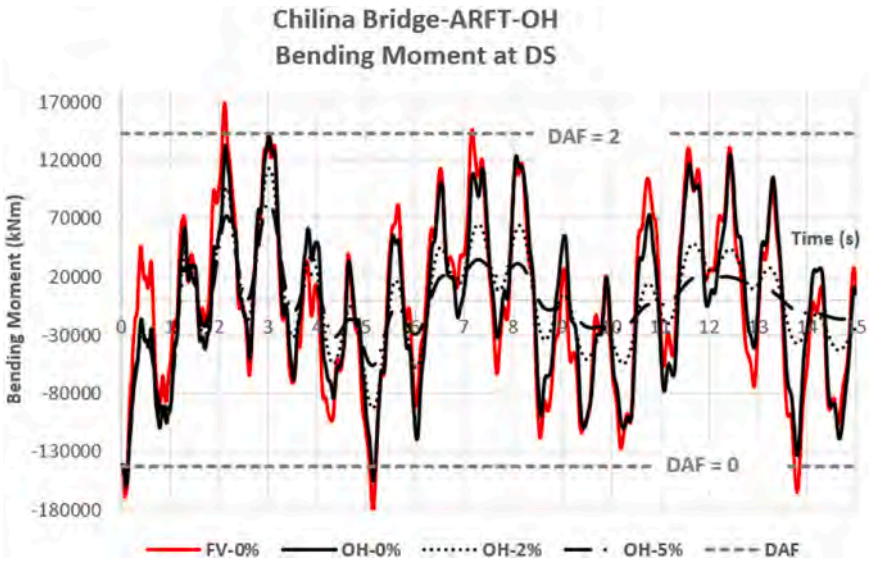

Fig. 29. Bending Moment vs Time diagram at section DS in case ARFT-OH over Chilina Bridge.

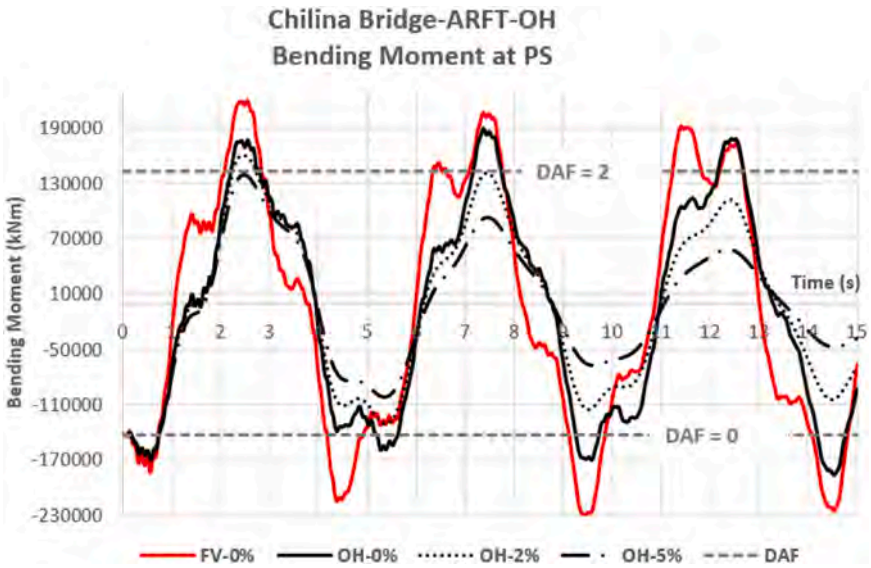

Fig. 30. Bending Moment vs Time diagram at section PS in case ARFT-OH over Chilina Bridge.

Table 1
Dynamic Amplification Factor (DAF) of Bending Moments.

Bridge	DAF							
	Type	FV	OH			US		
	Damping	**0%**	0%	2%	5%	0%	2%	5%
Bioceanic	IS/PS-B	**2.07**	1.95	1.84	**1.75**	1.98	1.91	**1.82**
	FS/DS-B	**7.93**	6.04	3.88	**3.05**	5.87	4.49	**3.80**
	FS/DS-F	**1.57**	1.46	1.25	**1.14**	1.38	1.25	**1.18**
	FS/PS-T	**2.27**	1.56	1.46	**1.38**	2.09	1.88	**1.78**
Chilina	DS	**2.18**	2.00	1.79	**1.58**	-	-	-
	PS	**2.54**	2.33	2.12	**1.97**	-	-	-

7. Conclusion

The results of the research into accidental release of the formwork traveller (ARFT) in bridge construction phases are shown in this article. The issue was approached from both the perspective of the simplified method as outlined in the regulations and from an experimental and numerical analysis standpoint to compare the results. For the experimental campaign, a scale model of more than 6 m length of the cable-stayed Bioceanic Bridge in the construction stage was built to perform the ARFT tests. Based on these tests, finite element models (FEM) were calibrated. That is to say the force that the deck of the bridge has to bear coming from the formwork traveller during the overturning process was

Table 2
Dynamic Reduction Factor (DRF) of Bending Moments.

Bridge	DRF								$OH_{5\%}$ / $US_{5\%}$
	Type	FV	OH			US			
	Damping	0%	0%	2%	5%	0%	2%	5%	
Bioceanic	IS/PS-B	1.00	0.89	0.78	**0.70**	0.92	0.85	**0.77**	**0.92**
	FS/DS-B	1.00	0.73	0.42	**0.30**	0.70	0.50	**0.40**	**0.73**
	FS/DS-F	1.00	0.81	0.43	**0.25**	0.67	0.44	**0.31**	**0.80**
	FS/PS-T	1.00	0.44	0.36	**0.30**	0.86	0.69	**0.62**	**0.49**
Chilina	DS	1.00	0.86	0.73	**0.63**	-	-	-	-
	PS	1.00	0.85	0.66	**0.49**	-	-	-	-

defined. Once it was calibrated, another critical stage from the ARFT viewpoint of the Bioceanic Bridge was analyzed by FEM. In order to study different bridge typologies, FEM analysis of ARFT was performed in a continuous beam bridge such as the Chilina Bridge. The main conclusions of the research are summarized in the following:

The regulations describe two approaches to address the problem of ARFT in bridge design: a simplified method based on considering a Dynamic Amplification Factor (DAF) relative to the static case equal to 2, or a specific dynamic analysis, for which they do not provide any guidance. The results of the analysis conducted in this article show that, depending on the selected damping value, bridge type, and construction phase, the DAF in critical sections can be significantly higher than 2 (reaching DAF=2.54) or clearly below (DAF=1.14). This is because bridges are multi-degree-of-freedom systems, and simplifying them to a single degree of freedom, as the simplified method in the regulations does, can sometimes lead to a loss of required accuracy. In other words, there are instances where the simplified method can either oversize or undersize a structure. For those cases where the regulations recommend a specific dynamic analysis, this research has developed a methodology that bridge design engineers can be easily applied in dynamic analyses.

The experimental tests performed in the research used a formwork traveller with modified mechanical properties compared to real formwork travellers (lower polar mass moment of inertia and larger eccentricity of the load). Based on this, the force-time functions obtained from experimental tests can be considered as conservative (lighter and shorter than real ones). These force-time functions with a rectangular shape achieve a good fit with experimental results and can be summarized according to the total self-weight dropped (SW_T) as follows: Regarding Overhead formwork travellers (OH) the force applied on the bridge can be assumed to be SW_T /3 during 0.9 s; while for Underslung formwork travellers (US) the force applied on the bridge can be assumed to be SW_T /5 during 0.5 s. These forces must be applied in the opposite direction to the movement produced by the initial static displacement (due to self-weight in balanced position before dropping). Dynamic calculations using these force functions to consider ARFT provide more accurate and reliable results than the simplified method proposed by regulations. Finally, a comparison between formwork OH and US travellers was performed. It is worth highlighting that the OH typology is safer than the US one from the point of view of ARFT because of the former, the internal forces on the bridge in the vibration process were reduced by between 8% and 51% depending on the section and phase.

The force-time functions described in this research have been obtained from experimental tests of the formwork traveller falling from a cable-stayed bridge and have been used for numerical models on other bridges, assuming that this function does not change significantly if the same formwork traveller were to fall from a different bridge. It would be interesting to experimentally verify this hypothesis through formwork traveller drop tests on other types of bridges in further research.

CRediT authorship contribution statement

Tommaso Argentini: Writing – review & editing, Supervision, Resources, Data curation. **Paula Pérez:** Visualization, Software. **Guillermo Capellán:** Resources, Project administration, Conceptualization. **Javier Sánchez-Haro:** Writing – original draft, Supervision, Methodology, Investigation, Formal analysis, Data curation, Conceptualization.

Declaration of Competing Interest

The authors declare that they have not known competing financial interests or personal relationships that could have appeared to influence the work reported in this paper.

Data availability

Data will be made available on request.

Acknowledgement

The authors would like to thank Arenas&Asociados for sharing the design drawings of the Bioceanic Bridge and the Chilina Bridge, based on which it was possible to consider the real static and dynamic behaviors of such relevant bridges. The authors would also like to thank the laboratory of Polytechnic of Milano for the quality of the experimental test performed.

Author agreement statement

We the undersigned declare that this manuscript is original, has not been published before and is not currently being considered for publication elsewhere.

We confirm that the manuscript has been read and approved by all named authors and that there are no other persons who satisfied the criteria for authorship but are not listed. We further confirm that the order of authors listed in the manuscript has been approved by all of us.

We understand that the Corresponding Author is the sole contact for the Editorial process. He/she is responsible for communicating with the other authors about progress, submissions of revisions and final approval of proofs.

References

[1] Eurocode 1: UNE-EN 1991-1–6.
[2] American Association of State Highway and Transportation Officials, AASHTO LRFD bridge specifications, 9th ed. 2020.
[3] Guide de conception:Ponts en béton precontraint constuirts par encorbellements successifs. Service d'Etudes techniques des routes et autoroutes (SETRA).Ministére de L'Equipament des Transports. France. 2003.
[4] Spanish regulation, Actions considered in railway bridges (IAPF-11),2012.
[5] Chopra AK. Dynamics of structures. Prentice Hall,; 1975.
[6] Sanchez- Haro J, Capellán G, Lombillo I. Equivalent static force in heavy mass impacts on structures. I J Struc Estab Dyn 2022;V.22(No 02). https://doi.org/10.1142/S0219455422500250.
[7] Sánchez-Haro J, Lombillo I, Capellán G. Simplified model to consider influence of gravity on impacts on structures: experimental and numerical validation. I J Impact Eng . 2023;vol. 173:104474. https://doi.org/10.1016/j.ijimpeng.2022.104474.
[8] Zhou HC, Li HN, Yang DH, Yi TH. Moving force identification of simply supported bridges through the integral time domain method. J Sound Vibrat 2022;534. https://doi.org/10.1016/j.jsv.2022.117046.

[9] Zhou L, Zhang J, Xu F. Efficient flexibility identification method using structured target rank approximation and extended Prony's method. J Sound Vibrat 2021; 509. https://doi.org/10.1016/j.jsv.2021.116254.
[10] Kar UK, Srinivas J. Free vibration and blast load analysis of porous functionally graded plates. Book: Compos materails Extrem Load 2022:519–33. https://doi.org/10.1007/978-981-16-4138-1_34.
[11] Lin X, Asraf M. Pressure–impulse response of semi-rigidly connected steel plates under blast loading. Int J Prot Struct 2017;8(1):25–7. https://doi.org/10.1177/2041419616663274.
[12] Li R, Kardomates GA, G.J.Simitses. Point-wise impulse (blast) response of a composite sandwich plate including core compressibility effects. Int J Solids Struct 2009;46(10):2216–23. https://doi.org/10.1016/j.ijsolstr.2009.01.036.
[13] Zhang H, Whang H, Xu Z, Liu Z, Gao H. Dynamic performance of ultra-long stay cable in small- scale extreme winds. Eng Struct 2023;290:116369. https://doi.org/10.1016/j.engstruct.2023.116369.
[14] Lee H, yoon H, Kim S. Vibration detection of stay-cable from low-quality CCTV images using deep-learning based dehazing and semantic segmentation algorithms. Eng Struct 2023;290:116567. https://doi.org/10.1016/j.engstruct.2023.116567.
[15] Li, H., Huang, Y., Guo E. "Construction Stage Seismic Resilience Evaluation of a Continuos Girder Bridge with the Cast-In-Place Catilever Method" Tehnicki Vjesnik, 30(4), 1010–1019, 2023. 10.17559/TV-20210929102016.
[16] Wang R, Hu Z, Hao Z, Chen L, Shi G, Hou R, et al. Seismic vulnebility analysis of long-span prestressed concrete composite box girder bridge with corrugated steel webs under construction. Buildings 2023;17(7):1598. https://doi.org/10.3390/buildings13071598.
[17] Jian B, Su Y, Li M. Buffeting response of cable-stayed bridge during construction under skew winds and pylon interference. KSCE J C Eng 2020;24(10):2971–9. https://doi.org/10.1007/s12205-020-1822-3.
[18] Xiong L, Cao H-Y, Tong Z-F, Xu K-L, Zhang C-T. Study on aerostatic instability of cable-stayed bridge with single tower in cantilever state. J Wuhan Univ Os Technol 2022;44(11):31–8. https://doi.org/10.3963/j.issn.1671-4431.2022.11.006.
[19] Wu F, Zhao L, Cao F, Ge Y. Numerical simulation anda validation of local wind enviroment of twin-box girder with wind barriers. Adv Bridge Eng 2023;4(1):13. https://doi.org/10.1186/s43251-023-00092-3.
[20] Wu X, Zhong B, Lv Y, Li ZX. Experimental study on dynamic amplification factor of simple-supported reinforced concrete beams under impact loading generated by an impulse hammer. 2150036 Int J Est Estab Dyn 2021;21(3):300–10. https://doi.org/10.1142/S021945542150036X.
[21] Tajima K, Inoue R, Hasuike R, Aso T. Calculation of dynamic response using eigenvectors in redundancy analysis of truss bridges. Appl Mech 2023;93(3):881–90. https://doi.org/10.1007/s00419-023-02365-9.
[22] S. Jeong H. Jung and K.C. Lee. Dynamic Amplification Assessment of high-speed railway Bridge Under Resonant responses using multi-sensor fusion, Proceeding of the internacional Congress on Sound and Vibration, 2023, ISBN 978–801103423-8.
[23] Sanchez-Haro J, Lombillo I, Capellan G. Modelling criteria proposal for dynamic analysis of beam bridges under moving loads using fem models. Structures 2023;50:651–69. https://doi.org/10.1016/j.istruc.2023.02.067.
[24] Zhang C, Lai Z, Yang X, Li Q, Zhang Z, Fu X. Dynamic analyses and simplified methods for evaluating complicated suspend-dome structures subjected to sudden cable failure. Int J Steel Struct 2023;23(1):18–36. https://doi.org/10.1007/s13296-022-00676-1.
[25] Chen Q, Wang H, EI-Tawil S, Agrawal AK, Bhattacharya B, Wong W. Behavior of a network tied-arch bridge subjected to sudden hanger loss scenarios. J Bridge Eng 2024;29(1):05023010. https://doi.org/10.1061/JBENF2.BEENG-6328.
[26] Martinez-Leal S, Osorio-Osorio D, Benjumea-Royero, Buelvas-Moya HA. Dynamic amplification factor due to sudden fall of the form traveler during the balanced cantilever construction of box girder bridges. Rev UIS Ing 2019;18(3):193–202. https://doi.org/10.18273/revuin.v18n3-2019020.
[27] Li X, Zhou J, Wu Y, Wang Z, Li X. Structural analyisis and improvement for a new form travellerin long-span cantilever-casting arch bridge. Adv Mech Engi 2021;13(4). https://doi.org/10.1177/16878140211009997.
[28] Zhao X, He S, Li Y, Yuan H. Process simulation of fore flucra form traveller construction for cable-stayed birdge. J Shenzhen Univ Sci Eng 2017;34(2):138–46. https://doi.org/10.3724/SP.J.1249.2017.02138.
[29] Capellan G, Sacristan M. Chilina Bridge over the Chili River in Arequipa. Balanced Cantilever segmental bridge in high seismicity area. 2017 IABSE Symp 2024:2110. https://doi.org/10.2749/222137814814068643. 2017.
[30] Nguyen DC, Salamak M, Katunin A, Gerges M. Finite element model updating of RC bridge structure with static load testing: a case study of vietnamese ThiThac bridge in coastal and marine environment. J Sens 2022;22(22):8884. https://doi.org/10.3390/s22228884.
[31] Hakim S, Konstantinovich D. Study of dynamic impact of speed trains on bridge structures. Int J Mech 2021;15:30–6. https://doi.org/10.46300/9104.2021.15.4.
[32] Grebowski K, Zielínska M. Dynamic analysis of historic railway bridges in Poland in the context of adjusting them to Pendolino trains. Int J Appl Mech Eng 2015;20(2):283–97. https://doi.org/10.1515/ijame-2015-0019.
[33] Sanchez-Haro J, Lombillo I, Capellan G. Modelling criteria proposal for dynamic analysis of beam bridges under moving loads using fem models. Structures 2023;50:651–69. https://doi.org/10.1016/j.istruc.2023.02.067.
[34] Diana G, Yamasaki Y, Larsen A, Rocchi D, Giappino S, Argentini T, et al. Construction stages of the long span suspension Izmit Bay Bridge: wind tunnel test assessment. J Wind Eng Ind Aerodyn 2013;123:300–10. https://doi.org/10.1016/j.jweia.2013.09.006.